Accelerated convergence of convective simulations using boundary value problems

Evan H. Anders and Benjamin P. Brown
Dept. Astrophysical & Planetary Sciences, University of Colorado – Boulder, Boulder, CO 80309, USA and Laboratory for Atmospheric and Space Physics, Boulder, CO 80303, USA

Jeffrey S. Oishi
Department of Physics and Astronomy, Bates College, Lewiston, ME 04240, USA

We present a method for using coupling Boundary value problems (BVPs) with Initial value problems (IVPs) in order to achieve thermally converged convective solutions on dynamical timescales, rather than the long thermal timescale. We demonstrate the similarity between the solution reached via BVP and the solution reached by a long thermal rundown of the IVP, and demonstrate that this method works at a large range of supercriticalities. We use this method to achieve converged solutions at high Ra, and discuss its extension to more complex scenarios, such as stratified, compressible convection.

I. TO DO

1. Get 3D cases in
2. Continue Improving Figures
3. Write figure captions
4. Think about post-bvp multiplying. Should it be a profile for both the velocity and for the T perturbations, rather than a scalar? I'm starting to think it should.

II. INTRODUCTION

Natural convection occurs in the presence of disparate timescales. Granules on the solar surface overturn on the order of 10 minutes, whereas deep motions in the Sun are likely at low Mach number and constrained by the solar rotation rate of $\sim$1 month. Despite these relatively short dynamical times, the scale of energy transport on the Sun occurs on the Kelvin-Helmholtz timescale of nearly 3×10^7 *years* [1]. As simulations aim to model natural convection by increasing into the high-Rayleigh Number (Ra) regime, where diffusive timescales are much longer than dynamical timescales [2], achieving converged simulations will require runs which span a greater number of convective timescales in order to thermally converge. Furthermore, with increasing Ra and decreasing diffusivities, motions become more turbulent and require finer grid meshes and smaller timesteps to resolve turbulent motions, meaning that achieving even one overturn timescale becomes a harder problem. These two effects combine such that achieving thermally converged, high-Ra, astrophysically interesting simulations is intractable using modern numerical tools.

In studies of stratified convection where a convective layer lies between stable layers, studies have used the knowledge of Mixing Length Theory (MLT) to adjust the initial thermal profile of atmospheres to a state which is closer to the adiabat chosen by convection [3]. However, many studies of convection do not contain stable layers above and below the convection zone, and the presence of hard boundaries and the boundary layers that they form makes it difficult to know proper evolved adiabat *a priori* before the dynamics of the simulation evolve the structure of the boundary layers.

Here we present a method for using simple boundary value problems (BVPs), along with information about the evolved flow fields, to fast-forward the slow thermal evolution of convecting simulations. We run two sets of experiments: one in which we allow convective simulations to evolve for a full thermal timescale before taking measurements, and another in which we employ a fast-forwarding, BVP technique which occurs on dynamical timescales. We compare these two sets of simulations to show the validity of the BVP technique. Then, we use the BVP technique to run simulations at high Ra, in the regime where running for thermal timescales becomes computationally intractable.

III. EXPERIMENT

In our study, we adopt the Oberbeck-Boussinesq approximation. Here, the fluid has constant kinematic viscosity (ν), thermal diffusivity (κ), and coefficient of thermal expansion (α). We non-dimensionalize length by the layer

height (L_z) , temperature by the (constant) initial temperature gradient across the layer (∇T_0), and time by the freefall timescale ($L_z/v_{\rm ff}$, with $v_{\rm ff} = \sqrt{\alpha g L_z^2 \nabla T_0}$, where g is uniform gravitational acceleration in the $-\hat{z}$ direction). The dimensionless Boussinesq equations governing the velocity $\boldsymbol{u} = u\hat{x} + v\hat{y} + w\hat{z}$, temperature $T = T_0 + T_1$, and reduced pressure ϖ are [4]

$$\nabla \cdot \boldsymbol{u} = 0, \tag{1}$$

$$\frac{\partial \boldsymbol{u}}{\partial t} + \boldsymbol{u} \cdot \nabla \boldsymbol{u} = -\nabla \varpi + T_1 \hat{z} + \frac{\rm Pr}{\rm Ra} \nabla^2 \boldsymbol{u}, \tag{2}$$

$$\frac{\partial T_1}{\partial t} + \boldsymbol{u} \cdot \nabla (T_0 + T_1) = \frac{1}{\rm Pr\,Ra} \nabla^2 T_1, \tag{3}$$

where the dimensionless control parameters are the Rayleigh and Prandtl numbers,

$$\mathrm{Ra} = \frac{g\alpha L_z^4 \nabla T_0}{\nu\chi} = \frac{(L_z\, v_{\rm ff})^2}{\nu\chi}, \qquad \mathrm{Pr} = \frac{\nu}{\chi}. \tag{4}$$

The dimensionless vertical extent of the domain is $z = [-1/2, 1/2]$, and at the boundaries we impose no-slip, impenetrable boundary conditions such that $w = u = v = 0$ at $z = \pm 1/2$. At the lower boundary, we employ a fixed flux condition such that $\partial T_1/\partial z = 0$ at $z = -1/2$, and we impose a fixed temperature condition $T_1 = 0$ at $z = 1/2$. Both horizontal directions are periodic, extending over a range $x, y = [0, \Gamma]$, where the aspect ratio is $\Gamma = 2$.

The chosen thermal boundary conditions at the upper and lower plates determine key quantities of the evolved state. Studies of incompressible, Boussinesq, Rayleigh-Bénard convection often employ fixed temperature (Dirichlet) or fixed heat flux (Neumann) boundary conditions at both plates. Dirichlet conditions represent plates of infinite conductivity, whereas Neumann conditions model plates of finite conductivity. In both cases, choosing symmetric boundary conditions maintains overall system symmetry, and despite evolving towards different thermal structures, both types of conditions transport heat in the same manner [5]. Studies of convection which aim to model astrophysical systems such as stars often employ a mixture of these two types of boundary conditions [6–8]. The flux at the lower boundary is fixed, modeling the constant energy generation of the stellar core, while the outer boundary condition is held at a fixed temperature, modeling the surface of a star which must output the energy generated internally. This setup is a useful model for understanding natural systems, but simulations which employ these boundary conditions suffer from a long thermal relaxation as the atmosphere loses energy and approaches the adiabat chosen by the Dirichlet condition. We choose these conditions in part to better understand them, and in part because these conditions minimize the number of assumptions that must be made in setting up the boundary value problem.

A. The Boundary Value Problem

The prohibitively long thermal timescale required to reach an equilibrium temperature profile in a Direct Numerical Simulation (DNS) can be skipped by coupling the DNS with a simple Boundary Value Problem (BVP) solve. Using information about the dynamics of the convection in the atmosphere, it is possible to skip a large portion of the thermal evolution, see Fig 1a&b.

The Boussinesq BVP contains equations of hydrostatic balance and thermal equilibrium,

$$\frac{\partial}{\partial z} \langle \varpi \rangle = \langle T_1 \rangle \hat{z}, \tag{5}$$

$$\frac{\partial}{\partial z} \langle w T_1 \rangle = \frac{1}{\rm PrRa} \frac{\partial^2}{\partial z^2} \langle T_1 \rangle, \tag{6}$$

where $\langle A \rangle$ represents a time- and horizontally averaged profile of the quantity A. These equations arise from taking time- and horizontal- averages of Eqns (2&3), neglecting terms that vanish due to symmetry, and assuming that the flows are in a stationary state. Convective flows are perturbations around a thermal profile defined by these equations in the proper evolved state.

Under eqns (5&6), the thermal structure ($\langle T_1 \rangle$, $\langle \varpi \rangle$) of the atmosphere is fully determined by the specification of the convective flux, $F_{conv} = \langle w T_1 \rangle$. If this profile is known, then solving for $\langle T_1 \rangle$ and $\langle \varpi \rangle$ depends only upon the choice of boundary conditions.

By definition, the profile of F_{conv} is *not* in its time stationary state near the beginning of the simulation. In fact, under mixed boundary conditions, as the atmosphere approaches the isotherm specified by the upper boundary condition, the motions display an asymmetric flux as energy leaks through the upper boundary condition (Fig. 1c). In order to construct the evolved convective flux from the current fluxes in the atmosphere, we acknowledge that the

evolved solution will be in flux equilibrium, carrying the amount of flux specified at the fixed-flux condition throughout the full depth of the atmosphere. Thus, the steady-state profile of the convective flux can be approximated as

$$F_{\text{conv, steady}} = F_{\text{bot}} \frac{\langle wT_1 \rangle}{\langle wT_1 - \kappa \partial_z (T_0 + T_1) \rangle} = F_{\text{bot}} \frac{\langle F_{\text{conv, IVP}} \rangle}{\langle F_{\text{tot, IVP}} \rangle}. \tag{7}$$

In essence, the construction of this profile assumes that the system appropriately picks out the ratios

$$f_{\text{conv}} = \frac{F_{\text{conv}}}{F_{\text{tot}}} \qquad f_{\text{cond}} = \frac{F_{\text{cond}}}{F_{\text{tot}}}. \tag{8}$$

in the transient state. Thus, even though the quantity of flux being carried is not correct, the system is carrying flux convectively where it needs to in the interior, and conductively in the boundaries.

The choice of a fixed-flux boundary condition at the bottom appropriately scales the magnitude of $F_{\text{conv, steady}}$. The choice of a fixed-temperature boundary condition at the top of the atmosphere appropriately sets the isotherm of the convective interior. While this method can be used for other choices of thermal boundary conditions (see Discussion), dual fixed temperature conditions at the upper plate require a more careful handling of F_{bot}, and dual fixed flux boundary conditions have degenerate solutions for the constant offset of T_1.

In general, the BVP solve takes the following form:

1. Run the convective IVP. Once the convection begins, start taking averages averages of $\langle wT_1 \rangle$ and $\partial_z^2 \langle T_1 \rangle$, which determine the fluxes through the system. Update these averages every $\Delta t = 0.1$ freefall times. Once these averages are converged to 1 part in 1000, the BVP is ready to be solved.

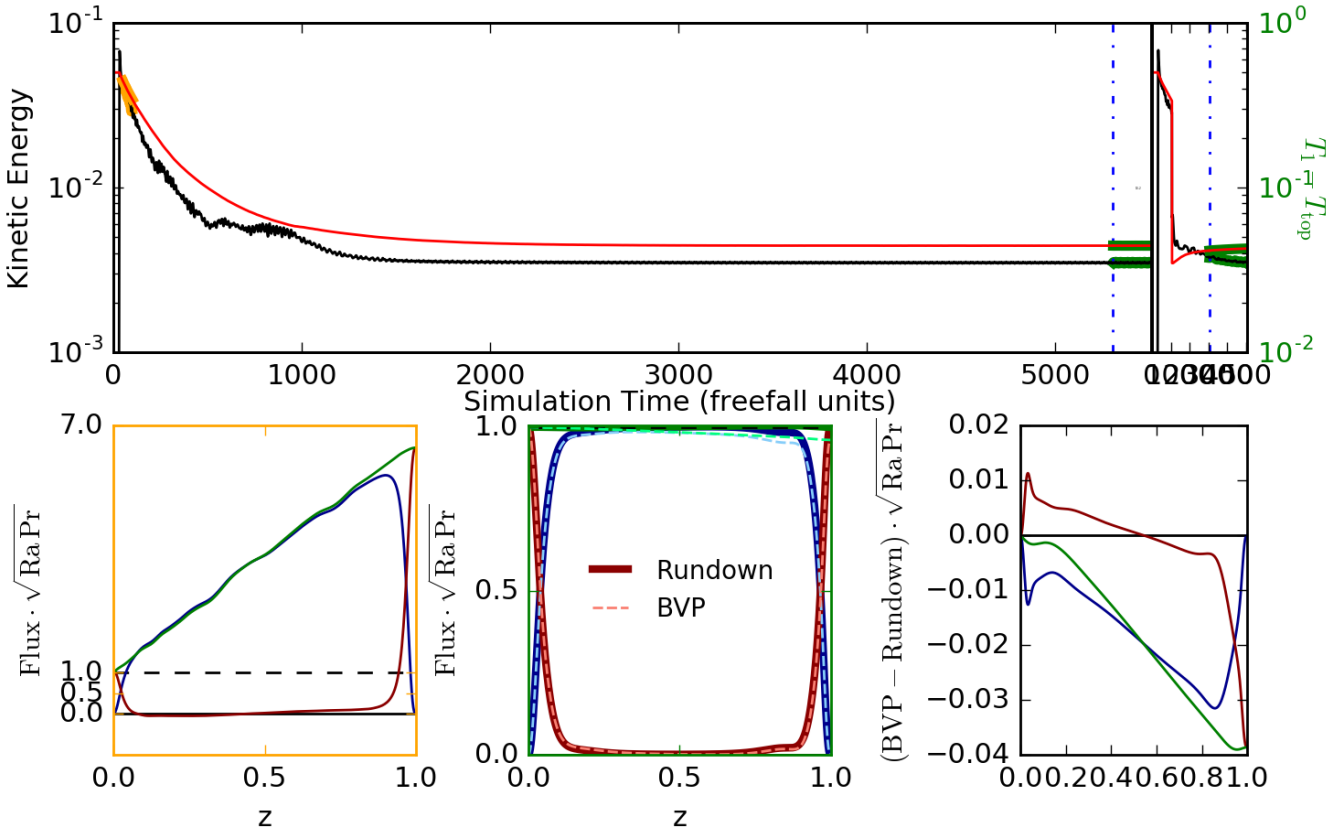

FIG. 1. Traces of system energies vs. time for a long thermal rundown (a) and BVP convergence (b) are shown for Ra = $1.30 \cdot 10^7$ ($S = 10^4$). The two plots are scaled such that one time unit on the x-axis of either run takes up an equivalent amount of space on the paper to illustrate the time savings of the BVP run. (c&d) Flux plots, where black is the sum of the flux, blue is enthalphy flux and red is condcutive flux. (c) Fluxes are shown for the IVP at an early time to illustrate the asymmetry of the flux through the system. (d) Fluxes through the converged, rundown state are compared to the fluxes in the converged BVP solution, where their difference is shown in (e).

2. Construct $F_{\text{conv, steady}}$ from the flux profiles, then use it to solve for $\langle T_1 \rangle$ and $\langle \varpi \rangle$ of the evolved state. Adjust the mean profiles in the BVP such that this is their mean profile.

3. Divide the velocities and the T_1 fluctuations around the mean profile by $\sqrt{F_{\text{bot}}/F_{\text{tot}}}$. This lowers the convective flux through the system such that it is, on average, the convective flux used in the BVP solve.

4. Continue running the IVP for a number of freefall times to allow the velocities and temperature perturbations to equilibrate to the new mean state.

This procedure seems to work quite well, see Fig. 1d&e.

B. Numerics

We utilize the Dedalus[1] pseudospectral framework [9] to time-evolve (1)-(3) using an implicit-explicit (IMEX), third-order, four-step Runge-Kutta timestepping scheme RK443 [10]. The temperature field is decomposed as $T = T_0(z) + T_1(x, y, z, t)$ and the velocity is $\boldsymbol{u} = w\hat{\boldsymbol{z}} + u\hat{\boldsymbol{x}} + v\hat{\boldsymbol{y}}$. In our 2D runs, $v = 0$. Variables are time-evolved on a dealiased Chebyshev (vertical) and Fourier (horizontal, periodic) domain in which the physical grid dimensions are 3/2 the size of the coefficient grid. Domain sizes range from 32x128 coefficients at the lowest values of Ra to 1024x4096 coefficients at Ra $> 10^9$ in 2D.

As initial conditions, we fill T_1 with random white noise whose magnitude is $10^{-6}(\text{Ra Pr})^{-1/2}$. This ensures that the initial perturbations are much smaller than the evolved convective temperature perturbations, even at large Ra. We filter this noise spectrum in coefficient space, such that only the lower 25% of the coefficients have power.

In 2D, there are often multiple steady state solutions (e.g., 2-roll and 3-roll solutions) which have slightly different flow properties (heat transport, etc.). Even though the initial perturbations are very small, they shape the convective transient and thus determine the nature of the steady state convection, at least in the laminar regime. In order to ensure that our results are not biased by differences in flow structure, we ran the simulations using distinct random temperature perturbations so as to compare statistics in comparable flow fields. In 3D, rolls are nonstationary over convective timescales, and so these effects need not be considered there.

IV. RESULTS

While the differences in the fluxes in Fig. 1 are small, it is important to determine if the velocity fluctuations and point-by-point nonlinear transport are the same in the evolved state. Fig. 2 overlays the probability distribution functions of the vertical and horizontal velocities, as well as the fully nonlinear portion of the convective flux for the same case as is shown in Fig. 1. The PDFs are quite similar visually, and have a similarity of (XYZ) according to a Kolmogorov-Smirnov statistic.

In addition to getting the nonlinear dynamics mostly correct, we show that the BVP method retrieves the proper temperature profile, see e.g., Fig. 3. Here the BVP profile retrieves the mean profile of the temperature to within 1% accuracy, and temperature fluctuations in the two runs have a similarity of (XYZ) according to a Kolmogorov-Smirnov statistic.

This method works across a broad range of supercriticality. In Fig. 4, we show measurements of the volume-averaged Nusselt number, Reynolds number, and temperature. We use standard definitions of the Nusselt number and Reynolds numbers,

$$\text{Nu} = \frac{\langle wT - (\text{Ra Pr})^{-1/2}\nabla T \rangle}{\langle -(\text{Ra Pr})^{-1/2}\nabla T \rangle} = 1 + \frac{\langle wT \rangle}{-\Delta T}\sqrt{\text{Ra Pr}}, \qquad \text{Re} = \frac{|\boldsymbol{u}|L_z}{\nu}, \tag{9}$$

where $\Delta T = T(z = 1/2) - T(z = -1/2)$ is the evolved temperature difference between the top and bottom plates. This form of the Nusselt number is valid even when the system is not yet in flux equilibrium, and reduces to the standard fixed flux definition of $\text{Nu} = [1 - \langle wT \rangle / P]^{-1}$ [5]. We find a scaling law of $\text{Nu} \propto \text{Ra}^{2/3}$, much steeper than a standard 2/7 or 1/3 scaling law [5]. Furthermore, we find that $\text{Re} \propto \text{Ra}^{0.425}$. The average temperature approaches the value at the top of the domain as Ra increases.

[1] http://dedalus-project.org/

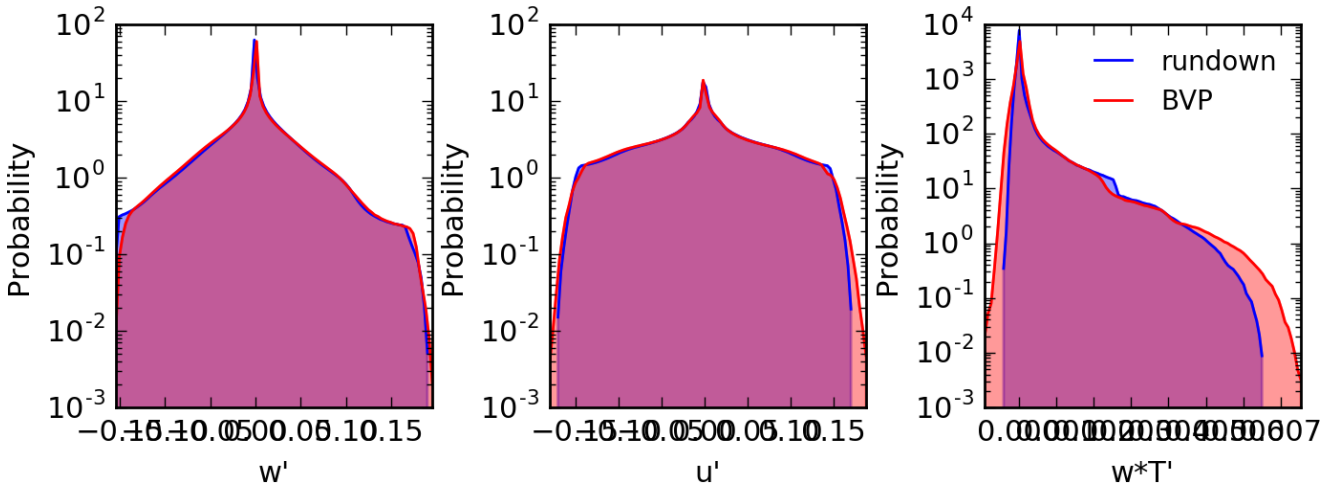

FIG. 2. We compare the time-variant dynamics in our 2D solutions by showing probability distribution functions of the values of vertical velocity (a), horizontal velocity (b), and nonlinear heat transport (c) in our converged solutions. The horizontal velocities are very similar, with a KS test similarity of X. The vertical velocities, too, are similar, with a KS similarity of Y. The nonlinear heat transport, while overall quite similar, shows that the BVP experiences a greater number of extreme events. The peak around zero for all three PDFs reflects the no-slip boundary conditions.

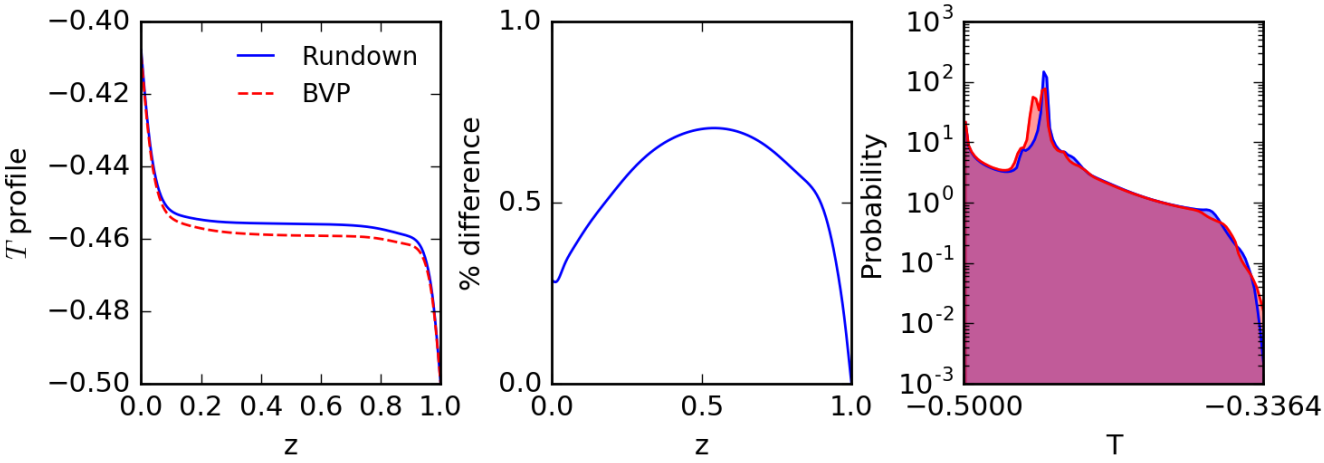

FIG. 3. Here we compare the evolved thermodynamic state of a BVP to that of a rundown IVP that has been run through a thermal timescale. (a) The temperature profiles, as a function of height, are shown. (b) The percentage difference between the temperature profiles, as a function of height, is shown. (c) PDFs comparing the values of the point-by-point temperatures over the averaging window. While the median of the PDF has a distinct offset between the two runs, the thermal fluctuations about the mean which drive the convection are nearly the same.

The final morphology of the flows is very important in determining the exact value of Nu and Re. In general, a two-roll state vs. a three-roll state will have entirely different statistics – different Nu, Re, and average temprature (and as a result, different size boundary layers). Thus, in 2D studies, it is essential to study flows of a similar morphology in order to see a clear trend.

V. DISCUSSION & CONCLUSIONS

While imperfect, the method presented here is a first step towards taking meaningful measurements of highly turbulent convection on manageable, human timescales. As demonstrated in Figs. 1-4, this BVP method quickly converges simulations to within a few percent of the true final state, while preserving the natural behavior of the

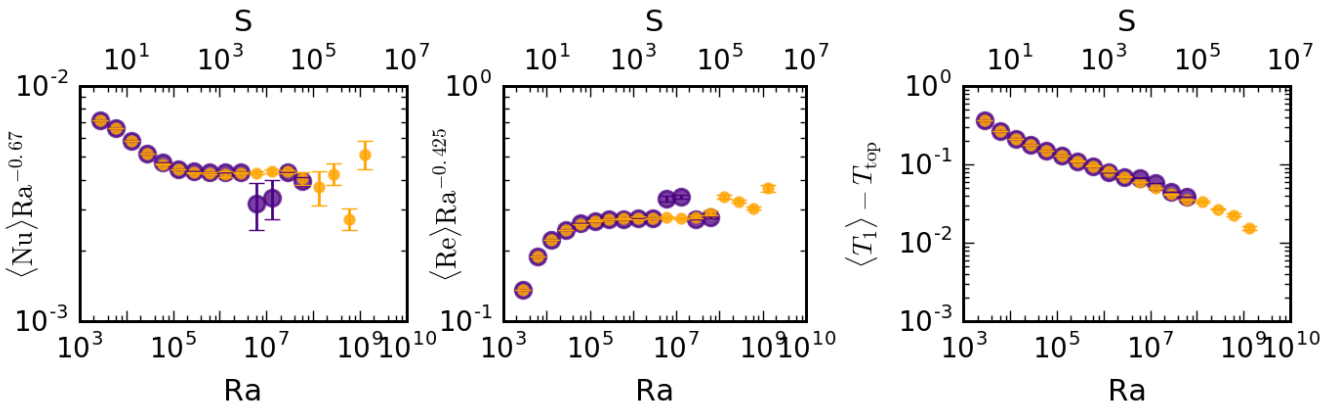

FIG. 4. Here we demonstrate the efficacy of the BVP method at many values of Ra. We show (a) Nusselt number scaling, (b) Reynolds number scaling, and (c) scaling of the mean temperature over the whole simulation. (a) The Nusselt number follows a classic 2/7 scaling law [5], until it reaches $\mathrm{S} = 10^{3+2/3}$, at which point the two-roll solution begins oscillating horizontally, showing time-variant Nu. The range of Nu over the averaging window is (blah), and the trend of Nu (the variance of the mean Nu) is shown as (blah). (b) Re follows an expected 1/2 scaling law. (c) The mean value of temperature, minus the value at the fixed-temperature boundary, is shown. As Ra increases, the boundary layers shrink, and the convection becomes more efficient, we anticipate this value to get closer and closer to zero as the atmosphere approaches the isotherm defined by the upper boundary.

convective solution (such as the oscillatory nature of high-Ra 2D states in 4).

While not perfect, the BVP method here has one major benefit over some of the other methods currently being used to achieve high Ra solutions. One oft-used method is that of bootstrapping, in which the converged solution of a low-Ra state is used as initial conditions for a higher-Ra simulation. While these methods are extremely powerful, they are influenced by hysteresis effects, and the powerful, steady rolls achieved at low Ra can result in an artifically over-stable high-Ra roll solution. The BVP method can be used with random noise initial conditions which allow the convective solution to be naturally chosen by the dynamics.

One benefit of the method presented here is that it can be easily extended to more complicated configurations. For example, to use this method in simulations of stratified compressible convection, one need only adapt the BVP equations to the appropriate equations of hydrostatic equilibrium, $\nabla P = -\rho \boldsymbol{g}$, and thermal equilibrium, $\nabla \cdot (F_{\mathrm{cond}} + F_{\mathrm{conv}}) = \mathrm{sources}$, for the problem at hand. In compressible convection, where the density is allowed to change, one must also use the knowledge of stellar structure codes and add an equation of mass conservation in order to ensure that the BVP does not spuriously add or remove mass from the system.

This method can be extended to other boundary conditions, as well. To solve for fixed temperature boundary conditions, the difficulty is in finding the amount of flux through the system – but this can be done by using the ratios f_{conv} and f_{cond}. In the case of fixed flux boundary conditions, there is degeneracy in the temperature solution which can come out of the BVP, but in using knowledge about the system – such as the initial symmetry of the RB state around $T_1 = 0$, the final solution can be pegged onto the proper profile.

ACKNOWLEDGMENTS

EHA acknowledges the support of the University of Colorado's George Ellery Hale Graduate Student Fellowship. This work was additionally supported by NASA LWS grant number NNX16AC92G. Computations were conducted with support by the NASA High End Computing (HEC) Program through the NASA Advanced Supercomputing (NAS) Division at Ames Research Center on Pleiades with allocations GID s1647 and GID g26133.

Appendix A: Table of Runs

Ra	Supercriticality	nz	nx	t_{therm}	$t_{\text{post BVP}}$	t_{avg}
$2.79 \cdot 10^3$	$10^{1/3}$	32	128	52.8	50	100
$6.01 \cdot 10^3$	$10^{2/3}$	32	128	77.6	50	100
$1.30 \cdot 10^4$	10^{1}	32	128	114	50	100
$2.79 \cdot 10^4$	$10^{1+1/3}$	32	128	167	50	100
$6.01 \cdot 10^4$	$10^{1+2/3}$	32	128	245	50	100
$1.30 \cdot 10^5$	10^{2}	64	256	360	100	100
$2.79 \cdot 10^5$	$10^{2+1/3}$	64	256	528	100	100
$6.01 \cdot 10^5$	$10^{2+2/3}$	64	256	776	100	100
$1.30 \cdot 10^6$	10^{3}	128	512	$1.14 \cdot 10^3$	100	200
$2.79 \cdot 10^6$	$10^{3+1/3}$	128	512	$1.67 \cdot 10^3$	200	200
$6.01 \cdot 10^6$	$10^{3+2/3}$	256	1024	$2.45 \cdot 10^3$	200	200
$1.30 \cdot 10^7$	10^{4}	256	1024	$3.60 \cdot 10^3$	200	200
$2.79 \cdot 10^7$	$10^{4+1/3}$	256	1024	$5.28 \cdot 10^3$	200	200
$6.01 \cdot 10^7$	$10^{4+2/3}$	256	1024	$7.76 \cdot 10^3$	200	200
$1.30 \cdot 10^8$	10^{5}	512	2048	$1.14 \cdot 10^4$	500	500
$2.79 \cdot 10^8$	$10^{5+1/3}$	512	2048	$1.67 \cdot 10^4$	500	500
$6.01 \cdot 10^8$	$10^{5+2/3}$	512	2048	$2.45 \cdot 10^4$	500	500
$1.30 \cdot 10^9$	10^{6}	1024	4096	$3.60 \cdot 10^4$	500	500

[1] M. Stix, "On the time scale of energy transport in the sun," Solar Physics **212**, 3–6 (2003).

[2] E. H. Anders and B. P. Brown, "Convective heat transport in stratified atmospheres at low and high Mach number," Physical Review Fluids **2**, 083501 (2017), arXiv:1611.06580 [physics.flu-dyn].

[3] A. Brandenburg, K. L. Chan, Å. Nordlund, and R. F. Stein, "Effect of the radiative background flux in convection," Astronomische Nachrichten **326**, 681–692 (2005), astro-ph/0508404.

[4] E. A. Spiegel and G. Veronis, "On the Boussinesq Approximation for a Compressible Fluid." Astrophys. J. **131**, 442 (1960).

[5] H. Johnston and C. R. Doering, "Comparison of Turbulent Thermal Convection between Conditions of Constant Temperature and Constant Flux," Phys. Rev. Lett. **102**, 064501 (2009), arXiv:0811.0401 [physics.flu-dyn].

[6] N. E. Hurlburt, J. Toomre, and J. M. Massaguer, "Two-dimensional compressible convection extending over multiple scale heights," Astrophys. J. **282**, 557–573 (1984).

[7] F. Cattaneo, N. H. Brummell, J. Toomre, A. Malagoli, and N. E. Hurlburt, "Turbulent compressible convection," Astrophys. J. **370**, 282–294 (1991).

[8] L. Korre, N. Brummell, and P. Garaud, "Weakly non-Boussinesq convection in a gaseous spherical shell," Phys. Rev. E **96**, 033104 (2017), arXiv:1704.00817 [physics.flu-dyn].

[9] K. Burns, G. Vasil, J. Oishi, D. Lecoanet, and B. Brown, "Dedalus: Flexible framework for spectrally solving differential equations," Astrophysics Source Code Library (2016), ascl:1603.015.

[10] U. M. Ascher, S. J. Ruuth, and R. J. Spiteri, "Implicit-explicit Runge-Kutta methods for time-dependent partial differential equations," Applied Numerical Mathematics **25**, 151–167 (1997).